Development of 50 krpm Ultra-High Speed IPMSM For EV traction

Ren Tsunata, Masaki Kimura, Masatsugu Takemoto, Jun Imai

Okayama University, Graduate School of Environmental, Life, Natural Science and Technology, Okayama, Japan

E-mail: tsunata@okayama-u.ac.jp

ABSTRACT: This paper develops an ultra-high-speed 50 krpm motor for traction applications. A typical IPMSM structure is used for the rotor in this paper. At ultra-high speeds, the winding structure has a large effect on winding losses. Hence, this paper investigates the AC loss of the winding. The AC loss includes the eddy current loss and circulating current loss in the winding. Additionally, the ultra-high speed raises concerns about the rotor's critical speed. Therefore, in this paper, the shaft of the developed motor is manufactured, and the critical speed is evaluated.

KEY WORDS: IPMSM, winding, traction motor, 50 krpm, eddy current loss.

1. INTRODUCTION

In recent years, the requirements for traction motors have become more diverse. For example, there is a need to reduce costs by using ferrite magnets, and to increase efficiency by using variable magnetic flux technology [1], [2]. In addition, when it comes to electric vehicles (EV), the requirements for traction motor vibration and torque ripple are also strict, so various studies are being reported [3], [4].

On the other hand, a recent trend is the increasing demand for miniaturization of electrical motors from the perspective of reducing resources. Increasing the rotational speed is an effective way to miniaturize electrical motors, so various high-speed motors are being considered [5]-[8]. Tractions motors are no exception, and studies are being conducted on increasing speed [9].

In this paper, we develop a traction motor with a maximum rotational speed of 50 krpm and describe issues that arise from increasing speed and countermeasures. The developed motor is a high-speed motor based on the motor for IONIQ5, a commercially available EV. First, this paper evaluates the effect of eddy current loss due to the winding structure, and then discuss circulating current. Finally, because there is a concern about critical speeds when increasing speed, this paper performs an evaluation by experiments on the developed motor.

2. WINDING DESIGN

Table 1 lists the required specifications for the base model of a commercially available EV (IONIQ5) and the target model developed in this paper. The maximum rotational speed of the developed motor is 50 krpm, more than three times larger than the base model's maximum rotational speed of 15 krpm. The output power is constant at 160 kW, but the maximum torque of the developed motor is smaller due to the increased rotational speed. As a result, it is possible to reduce the size of the motor even with the same output power. In addition, the maximum current and battery voltage are the same for both models to make them easier

Table 1. Target specifications of 50 krpm IPMSM.

	Basic model*	Target model
Max. rotational speed	15,000 rpm	50,000 rpm
Max. torque	350 Nm	105 Nm
Output power	160 kW	160 kW
DC-bus voltage	697 V	697 V
Max. inverter current	240 Arms**	240 Arms

(*Traction motor mounted on IONIQ5) (**estimated value)

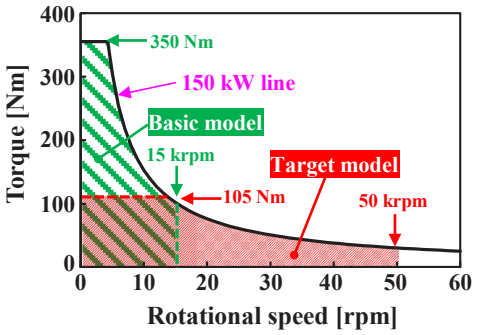

Fig. 1. Difference of operating area between basic model (IONIQ5) and a target motor (50 krpm).

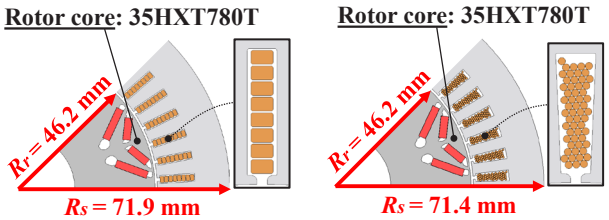

(a) Rectangular copper wire (b) Round copper wire

Fig. 2. Cross-sectional views of 50 krpm models employing different winding.

Table 2. Main parameters of three comparative models.

	Basic model (IONIQ5)	Target model (50 krpm) Hairpin	Round
Stator outer radius *Rs*	100 mm	71.9 mm	71.4 mm
Rotor outer radius *Rr*	66 mm	46.2 mm	46.2 mm
Rotor radius ratio *k*	1.0	0.7	0.7
Stack length	153 mm	160 mm	160 mm
Airgap length	0.8 mm	0.8 mm	0.8 mm

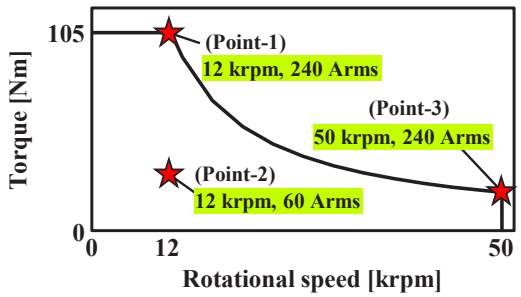

Fig. 3. Representative operating points of the developed motor.

to compare. Fig. 1 clearly visualizes the difference in the operating range of the two models.

Fig. 2 shows the cross sections of the developed 50 krpm models. Each model uses a different winding structure, using rectangular copper wire and round copper wire. The rotors have exactly the same structure, and use an interior permanent magnet (IPM) structure. The permanent magnet material used is NdFeB magnets, which are common in traction motors [10]. The stator core uses a typical laminated steel sheet, but the rotor core uses high tensile steel sheet. The parameters of both models shown in Fig. 2 are listed in Table 2.

Fig. 3 shows three typical operating points for comparing the losses of both models. Point-1 is the maximum torque point near the base speed. Point-2 is in the light load region near the base speed, which is an operating point frequently used in traction motors [11], [12]. Point-3 is the operating point with maximum speed and maximum output power.

Fig. 4 is a graph comparing the loss and efficiency of both models at the three representative operating points. At Point-1 in Fig. 4(a), the torque is maximum, so the copper loss of the winding is the largest. In addition, the magnetic flux amount is also maximum, so the iron loss in the stator core is also large. At Point-2 in Fig. 4(b), the current is smaller than Point-1, so the copper loss decreases and the iron loss in the stator core is maximum. At Points-1 and -2, the rotational speed is small, and hence the eddy current loss of the winding is small, and the efficiency difference due to the winding structure is not very large. However, at Point-3 in Fig. 4(c), the rotational speed increases to 50 krpm. As a result, the eddy current loss generated in the winding is large. Accordingly, the efficiency of the rectangular wire model is significantly reduced. Fig. 5 shows the current density distribution

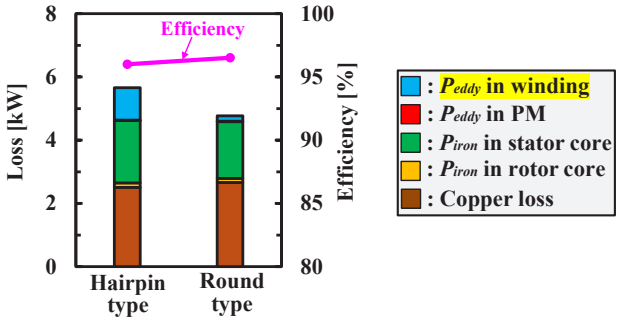

(a) Point-1 (12 krpm, 240 Arms)

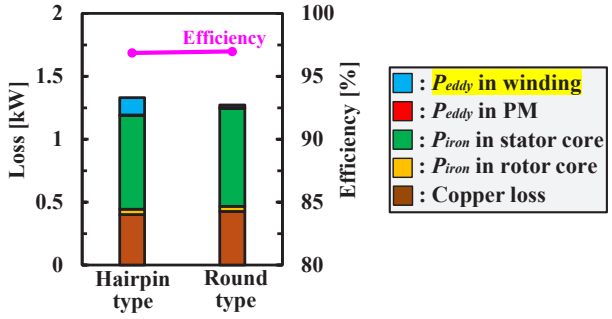

(b) Point-2 (12 krpm, 60 Arms)

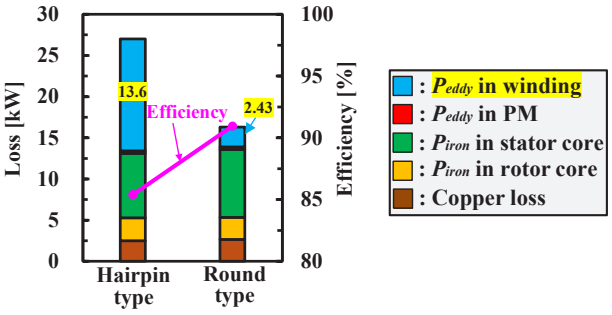

(c) Point-3 (50 krpm, 240 Arms)

Fig. 4. Loss, efficiency of target models using different winding at three operating points.

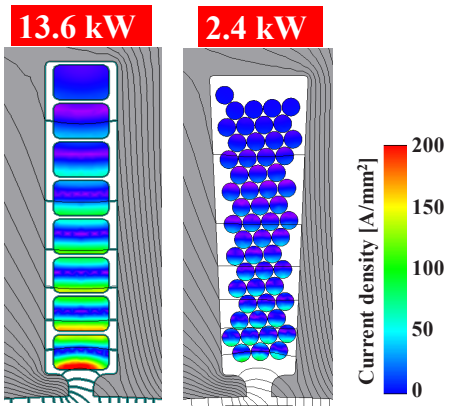

Fig. 5. Current density distributions of two models at Point-3.

Table 3. Winding parameters of five comparative models.

	φ0.5 mm	φ0.6 mm	φ0.7 mm	φ0.85 mm	φ0.95 mm
No. of turns	8	8	8	8	8
No. of parallel wire	14	10	7	5	4
Current density [Arms/mm^2]	21.8	21.2	22.3	21.1	21.2

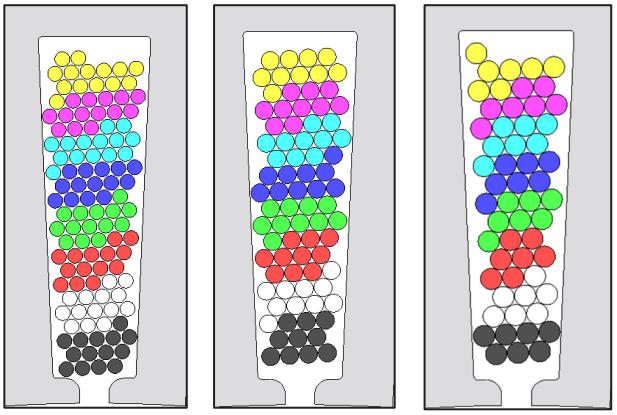

(a) φ0.5 mm (b) φ0.6 mm (c) φ0.7 mm

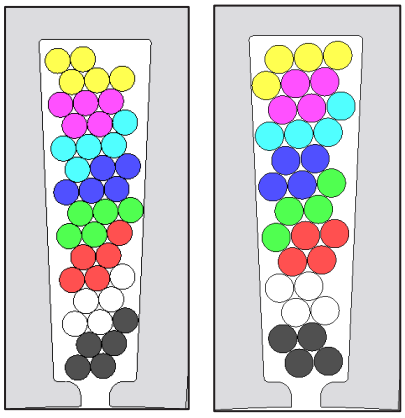

(d) φ0.85 mm (e) φ0.95 mm

Fig. 6. Cross-sectional views of five comparative models having different winding.

in the winding at Point-3 of both models. In the rectangular wire model, the eddy current loss is large, especially in the winding on the air gap side. At 50 krpm, the eddy current loss of the winding can be reduced by 82.4% by using round copper wire.

3. AC LOSS INCLUDING CIRCULATING CURRENT

Although the use of round copper wires can reduce the eddy current loss, circulating current loss between strands becomes an issue [13), (14)]. Therefore, in this paper, the circulating current loss is also evaluated.

As shown in Table 3 and Fig. 6, five patterns with different winding diameters are investigated. The parameters are determined so that the winding space factor is about 50% in all models.

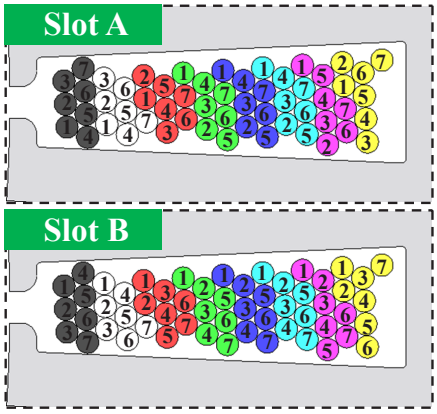

(a) Pattern-1

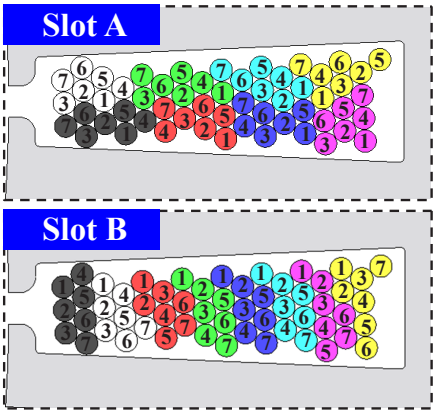

(b) Pattern-2

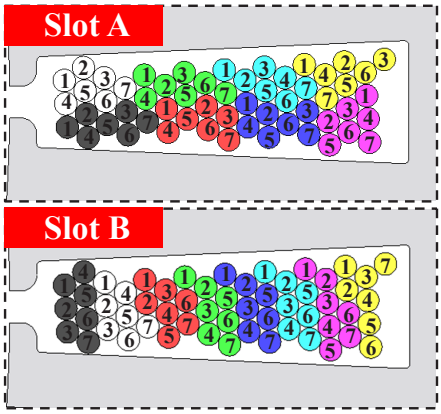

(c) Pattern-3

Fig. 7. Winding arrangement patterns for comparison.

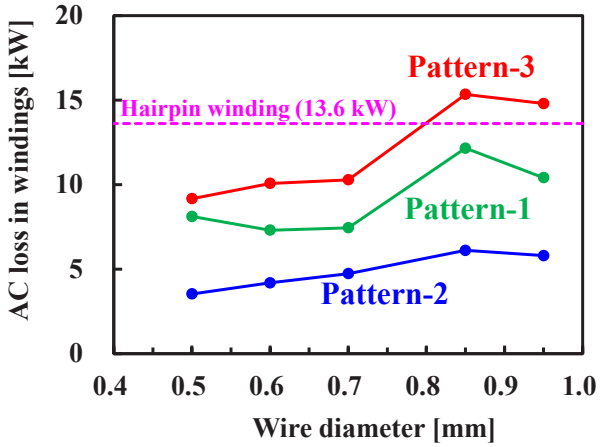

Fig. 8. AC loss in winding of five models at Point-3.

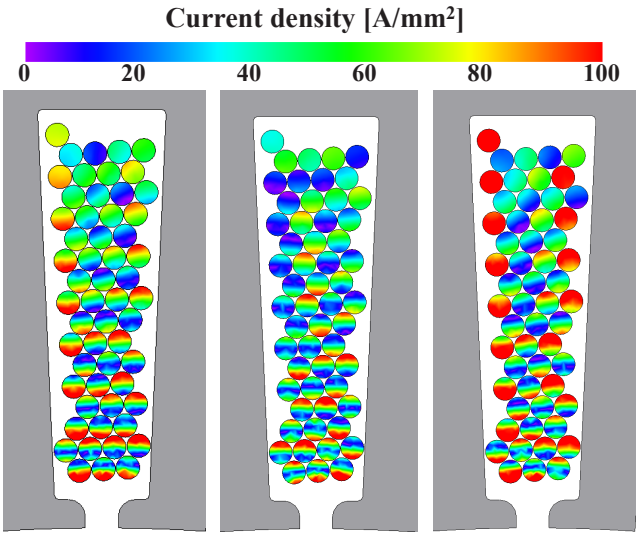

(a) Pattern-1 (b) Pattern-2 (c) Pattern-3

Fig. 9. Current density distributions of each winding arrangement when wire diameter is 0.7 mm at Point-3.

In addition, to evaluate the effect of circulating current when the winding arrangement is changed, analysis is performed for three patterns in which the winding arrangement is changed, as shown in Fig. 7. Patterns 2 and 3 can be achieved by twisting the winding at the coil end.

Fig. 8 shows the AC loss of the winding at Point-3 at the maximum speed. For all winding diameters, Pattern-2 has the largest AC loss. Since the eddy current loss is the same for the three winding arrangement patterns, this means that the circulating current loss has increased. Pattern-2 has a larger circulating current loss than Pattern-1, in which the coil ends are not twisted. On the other hand, Pattern-3 has the smallest AC loss for all models. As a result, it is possible to reduce the total loss, including circulating current loss, compared to the rectangular wire model.

Fig. 9 shows the current density distribution for each winding arrangement pattern when the winding diameter is 0.7 mm. In Pattern-3, which has the largest AC loss, it can be seen that a large current is also generated in the winding on the back yoke side due to circulating current. In addition, the current density in Pattern-2, which has the smallest AC loss, approaches the distribution in Fig. 5, which considers only eddy current loss.

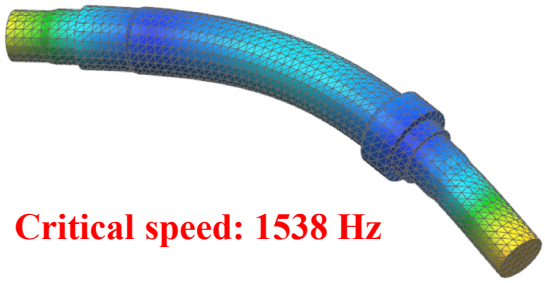

Fig. 10. Von Mises Stress distributions at maximum speed.

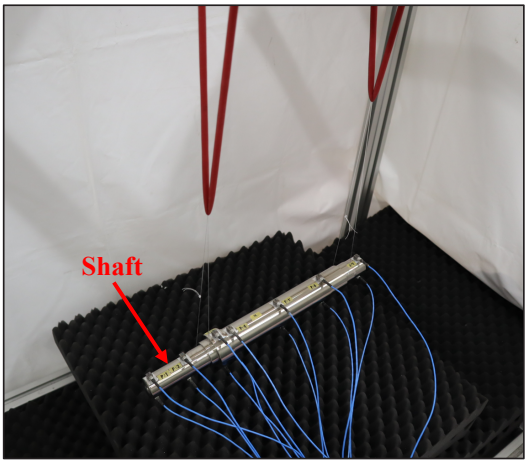

(a) Pattern-1

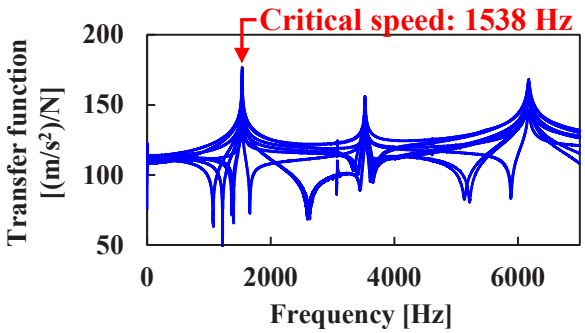

(b) Pattern-1

Fig. 11. Von Mises Stress distributions at maximum speed.

4. CRITICAL SPEED

For high-speed motors, it is necessary to evaluate the critical speed [15), (16)]. Fig. 10 shows the result of eigenvalue analysis of the shaft of the designed motor, with the critical speed being 1538 Hz.

Meanwhile, Fig. 11 shows the results of measuring a prototype shaft. Fig. 11(a) shows the test setup, and Fig. 11(b) shows the experimental result. In the experimental result, the critical speed is 1538 Hz, which is in perfect agreement with the analysis result. In addition, since 1538 Hz corresponds to 69.5 krpm, the safety factor for the maximum speed of the developed motor, 50 krpm, is 1.38.

5. CONCLUSIONS

In this paper, we designed a 50 krpm ultra-high-speed traction motor and clarified the appropriate winding structure and countermeasures against circulating current. Because the rotation speed is high, using rectangular wire would be thermally infeasible due to the large eddy current loss. The use of round wire has an eddy current suppression effect of more than 80%. We also clarified at 50 krpm that the circulating current is highly dependent on the winding arrangement. By using an appropriate winding arrangement, it is possible to reduce the total loss, including circulating current loss, compared to rectangular wire. The critical speed of the developed motor was also evaluated, and experiments confirmed that there were no operational problems.

ACKNOWLEDGMENT

This paper is based on results obtained from a subcontract from Transmission Research Association for Mobility Innovation (TRAMI) as part of the New Energy and Industrial Technology Development Organization (NEDO) Feasibility Study Program on Energy and New Environmental Technology / Resource saving of electric drive system for automobiles by ultra-high rotation of e-motor.(JPNP14004)

REFERENCES

(1) Y. -H. Jung, M. -R. Park, K. -O. Kim, J. -W. Chin, J. -P. Hong and M. -S. Lim, "Design of High-Speed Multilayer IPMSM Using Ferrite PM for EV Traction Considering Mechanical and Electrical Characteristics," in *IEEE Transactions on Industry Applications*, vol. 57, no. 1, pp. 327-339, Jan.-Feb. 2021, doi: 10.1109/TIA.2020.3033783.

(2) R. Tsunata, M. Takemoto, S. Ogasawara and K. Orikawa, "Variable Flux Memory Motor Employing Double-Layer Delta-Type PM Arrangement and Large Flux Barrier for Traction Applications," in *IEEE Transactions on Industry Applications*, vol. 57, no. 4, pp. 3545-3561, July-Aug. 2021, doi: 10.1109/TIA.2021.3068329.

(3) Z. Chen, B. Yang, Y. Lu, J. Li and K. Yang, "Torsional Vibration Analysis of Interior Permanent Magnet Synchronous Motors With Rotor Step-Skewing for Electric Vehicles," in *IEEE Transactions on Transportation Electrification*, vol. 10, no. 3, pp. 5250-5259, Sept. 2024.

(4) R. Tsunata and M. Takemoto, "Skewing Technology for Permanent Magnet Synchronous Motors: A Comprehensive Review and Recent Trends," in *IEEE Open Journal of the Industrial Electronics Society*, vol. 5, pp. 1251-1273, 2024, doi: 10.1109/OJIES.2024.3491295.

(5) S. -I. Kim, Y. -K. Kim, G. -H. Lee and J. -P. Hong, "A Novel Rotor Configuration and Experimental Verification of Interior PM Synchronous Motor for High-Speed Applications," in *IEEE Transactions on Magnetics*, vol. 48, no. 2, pp. 843-846, Feb. 2012.

(6) G. -H. Jang, J. -H. Ahn, B. -O. Kim, D. -H. Lee, J. -S. Bang and J. -Y. Choi, "Design and Characteristic Analysis of a High-Speed Permanent Magnet Synchronous Motor Considering the Mechanical Structure for High-Speed and High-Head Centrifugal Pumps," in *IEEE Transactions on Magnetics*, vol. 54, no. 11, pp. 1-6, Nov. 2018.

(7) D. -K. Hong, B. -C. Woo, J. -Y. Lee and D. -H. Koo, "Ultra High Speed Motor Supported by Air Foil Bearings for Air Blower Cooling Fuel Cells," in *IEEE Transactions on Magnetics*, vol. 48, no. 2, pp. 871-874, Feb. 2012.

(8) Y. Chen, B. Zang, H. Wang, H. Liu and H. Li, "Composite PM Rotor Design and Alternating Flux Density Harmonic Component Analysis of a 200 kW High-Speed PMSM Used in FESS," in *IEEE Transactions on Industry Applications*, vol. 59, no. 2, pp. 1469-1480, March-April 2023.

(9) T. -A. Huynh, P. -H. Chen and M. -F. Hsieh, "Analysis and Comparison of Operational Characteristics of Electric Vehicle Traction Units Combining Two Different Types of Motors," in *IEEE Transactions on Vehicular Technology*, vol. 71, no. 6, pp. 5727-5742, June 2022.

(10) J. Pyrhönen *et al*., "Hysteresis Losses in Sintered NdFeB Permanent Magnets in Rotating Electrical Machines," in *IEEE Transactions on Industrial Electronics*, vol. 62, no. 2, pp. 857-865, Feb. 2015.

(11) S. Benharref, V. Lanfranchi, D. Depernet, T. Hamiti and S. Bazhar, "Fast Computational Method for PWM Strategy Comparison of Machine and Inverter Electrical Losses: Application on WLTC Cycle," in *IEEE Transactions on Industrial Electronics*, doi: 10.1109/TIE.2024.3482006.

(12) R. Tsunata, M. Takemoto, J. Imai, T. Saito and T. Ueno, "Superior Efficiency Under PWM Harmonic Current in an Axial-Flux PM Machine for HEV/EV Traction: Comparison

With a Radial-Flux PM Machine," in *IEEE Transactions on Industry Applications*, vol. 60, no. 5, pp. 6736-6751, Sept.-Oct. 2024.

(13) Y. Yu, D. Liang, Z. Liang and Q. Ze, "Calculation for stator loss of high-speed permanent magnet synchronous machine in torque-speed envelope and restraint approach for circulating current in windings," in *CES Transactions on Electrical Machines and Systems*, vol. 2, no. 2, pp. 211-219, June 2018.

(14) L. Yang, T. Gao, C. Ai and X. Kong, "Thermal Analysis of Stator Iron-Core-Less PMBLDC Motors Considering Both Winding Eddy and Circulating Current Losses," in *IEEE Access*, vol. 12, pp. 49791-49803, 2024.

(15) J. Che *et al*., "Mechanical Field Calculation and Analysis of a High-Speed PMSM," in *IEEE Transactions on Magnetics*, vol. 60, no. 12, pp. 1-5, Dec. 2024.

(16) D. -K. Hong, J. -H. Choi, D. -J. Kim, Y. -D. Chun, B. -C. Woo and D. -H. Koo, "Development of a High Speed Induction Motor for Spindle Systems," in *IEEE Transactions on Magnetics*, vol. 49, no. 7, pp. 4088-4091, July 2013.